Appl. Phys. B 52, 122–131 (1991)

Applied Physics B Photophysics and Laser Chemistry

Polarization of Emission Spectra from Ti^{3+}-Doped Oxide Crystals

I. Molecular Orbital Theory

M. Yamaga[1], B. Henderson[2], and K. P. O'Donnell[2]

[1] Department of Physics, Faculty of General Education, Gifu University, Gifu 501-11, Japan

[2] Department of Physics and Applied Physics, University of Strathclyde, Glasgow, G4 0NG, Scotland, U.K.

Received 10 August 1990/Accepted 18 September 1990

Abstract. The photoluminescence spectra of Ti^{3+}-doped $YAlO_3$, $Y_3Al_5O_{12}$ and Al_2O_3 crystals display weak zero-phonon lines and broad vibronic side bands. The zero-phonon lines are due to the splitting of the $^2T_{2g}$ ground state into three Kramers' doublets by the combined effects of static axial crystal field, Jahn-Teller effect and spin-orbit interaction. A molecular orbital method is used to calculate the relative intensities and polarizations of both zero-phonon lines and broad band in terms of the mixing of odd-parity ligand wavefunctions into even-parity Ti^{3+} wavefunctions by odd-parity crystal fields of T_{1u} and T_{2u} symmetries at sites with tetragonal and trigonal symmetries. The odd-parity distortions may be static or dynamic and are of crucial relevance in determining the strength of vibronically induced transitions. In general, selection rules for optical spectra are uniquely determined by group theory. The relevance of the molecular orbit description of the d–d transitions is that it permits a physical interpretation of the strength of optical spectra in terms of the covalent charge transfer from ligand ions to central ions induced by odd-parity crystal field distortion.

PACS: 42.55R, 42.70, 79.60

Since the first demonstration of tunable room-temperature laser action at near infrared wavelengths from Cr^{3+}:$BeAl_2O_4$ [1], several other tunable Cr^{3+} lasers have been developed, using $Gd_3Sc_2Ga_3O_{12}$ (GSGG) [2]. $Gd_3Sc_2Al_3O_{12}$ (GSAG) [3], $ScBO_3$ [4], $ZnWO_4$ [5] and $KZnF_3$ [6] as host crystals. The Ti^{3+}:Al_2O_3 laser [7, 8] has an even broader tuning range and a much larger stimulated emission cross-section $\sigma_0 = 3 \times 10^{-19}\,cm^2$ at the luminescence peak [9] than Cr^{3+}-doped laser materials irrespective of whether the lowest excited state of Cr^{3+} is ^2E or $^4T_2$. Although the optical absorption and luminescence and excited state decay times of Ti^{3+} in $YAlO_3$ (YAP) [10], $Y_3Al_5O_{12}$ (YAG) [11] are comparable to those of Al_2O_3 [12–16], efficient laser operation has been observed only in Al_2O_3 crystals. In seeking novel Ti^{3+}-doped crystals for use as tunable lasers with high gain and large slope efficiency, it is instructive to examine the vibronic nature of the radiative $^2E_g \leftrightarrow {}^2T_{2g}$ transitions. This paper analyzes the zero-phonon line and broad-band emission of Ti^{3+} ions in axial crystal fields in terms of a molecular orbital method in which odd-parity ligand ion wavefunctions are mixed into the even-parity ^2E_g and $^2T_{2g}$ states of the $3d^1$ configuration by odd-parity crystal field distortions, spin-orbit coupling and Jahn-Teller interaction acting in concert. We derive the relative intensities and polarizations of the three zero-phonon lines and broadband in emission for Ti^{3+} ions in tetragonal or trigonal crystal field symmetry. These theoretical results will be compared to the low temperature emission spectra of Ti^{3+} in YAP, YAG and Al_2O_3 crystals in a subsequent publication.

1. Vibronic Hamiltonian of the $3d^1$ Configuration of Ti^{3+}

We consider the Ti^{3+} ion located at the centre of an octahedral array of anions which undergoes an axial distortion to produce in a crystal field with tetragonal or trigonal symmetry. The vibronic Hamiltonian for the $3d^1$ configuration of the Ti^{3+} ion in this axially distorted environment is written as

$$H = H_0 + H_{ph} + H_{s\text{-}o} + V_{ax} + V_{e\text{-}p}, \tag{1}$$

$$V_{ax} = \sum_{\Gamma,\gamma} V(\gamma(\Gamma)), \tag{2}$$

where the zero-order electronic Hamiltonian, H_0, includes both central ion and octahedral crystal field terms, V_0.

Table 1. Tetragonal and trigonal crystal field components for various symmetry groups

Symmetry group		Components
Tetragonal	D_{4h}	$V(A_{1g}(E_g))$
	C_{4v}	$V(A_{1g}(E_g)) + V(A_{2u}(T_{1u}))$
	C_4	$V(A_{1g}(E_g)) + V(A_{2g}(T_{1g})) + V(A_{1u}) + V(A_{1u}(E_u)) + V(A_{2u}(T_{1u}))$
Trigonal	D_{3d}	$V(A_{1g}(T_{2g}))$
	D_3	$V(A_{1g}(T_{2g})) + V(A_{1u}) + V(A_{1u}(T_{2u}))$
	C_{3v}	$V(A_{1g}(T_{2g})) + V(A_{2u}) + V(A_{2u}(T_{1u}))$
	C_3	$V(A_{1g}(T_{2g})) + V(A_{2g}) + V(A_{1u}) + V(A_{2u}) + V(A_{2u}(T_{1u})) + V(A_{1u}(T_{2u}))$

The symbols in parentheses represent the components of irreducible representations of D_{4h} and D_{3d} symmetry groups

The phonon Hamiltonian, H_{ph}, contains kinetic energy and harmonic potential energy terms. H_{s-o} and V_{e-p} are perturbation operators representing spin-orbit and electron-phonon interactions, respectively. $V(\gamma(\Gamma))$ in (2) is the component of the crystal field perturbed from cubic symmetry, V_{ax}, in which Γ and γ are irreducible representations of the group and its component. Table 1 summarizes these components of the tetragonal and trigonal static crystal field, $V(\gamma(\Gamma))$, for various symmetry groups. The even-parity crystal field components, $V(A_{1g}(E_g))$ for D_{4h} and $V(A_{1g}(T_{2g}))$ for D_{3d} correspond to the octahedron being distorted along the $\langle 001\rangle$ and $\langle 111\rangle$ axes, respectively. Lower symmetry distortions introduce odd-parity components which break the parity-forbidden selection rule for $d \leftrightarrow d$ transitions. The electron-phonon coupling operator, V_{e-p}, includes the Jahn-Teller effect and odd-parity perturbations, i.e. both static and dynamic distortions.

$YAlO_3$ is orthorhombic in symmetry. However, the octahedron surrounding Ti^{3+} may be treated as approximately tetragonal. A reduction of symmetry from tetragonal to orthorhombic introduces an odd-parity crystal field component, $V(A_{2u}(T_{1u}))$. In YAG Ti^{3+} substitutes for the Al^{3+} ion in the trigonally distorted octahedral sites in which the centre of inversion is maintained. As a consequence, the crystal field contains only even-parity components. In contrast, as the symmetry of Al_2O_3 is C_3, odd-parity components, $V(A_{2u}(T_{1u}))$ and $V(A_{1u}(T_{2u}))$, are present. Which components are dominant may be determined experimentally.

Figure 1 shows how the five-fold degenerate orbital state, ^2D, of Ti^{3+} in Al_2O_3 splits into ^2E_g and $^2T_{2g}$ levels [12] with energy separation, $10Dq$ [17]. The dominant static trigonal crystal field, $V(A_{1g}(T_{2g}))$, and spin-orbit interaction together splits the $^2T_{2g}$ ground state into Kramers' doublets, $E^2_{1/2}$, ($E^1_{1/2}$, $E_{3/2}$), which are representations of the trigonal double group [13, 17], whereas the ^2E_g excited state splits into two Kramers' doublets as a consequence of the Jahn-Teller effect. The optical spectra of Ti^{3+} in Al_2O_3 may be accounted for in terms of this schematic energy level diagram. In absorption, there are two overlapping peaks, the separation between which yields the Jahn-Teller splitting in the excited state of about $3000\,cm^{-1}$ [18]. At low temperature, high resolution measurements reveal a single zero-phonon line (transition A). In emission there are three zero-phonon

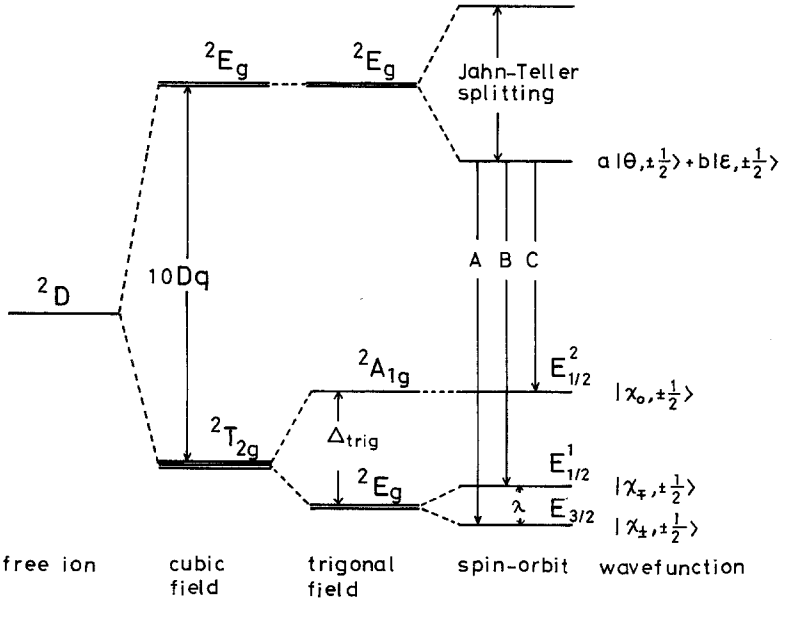

Fig. 1. Energy-level diagram of Ti^{3+}:Al_2O_3 including crystal field, spin-orbit interactions and the Jahn-Teller effect

lines due to the ground state being split into three Kramers' doublets. These absorption/emission transitions are allowed by the odd-parity crystal field components in Table 1 and odd-parity terms of $V_{e\text{-}p}$ in (1).

We now proceed to calculate the relative transition probabilities and polarizations of the zero-phonon emission lines and of the vibronically broadened band in terms of the odd-parity wavefunctions of the ground and excited states of Ti^{3+} ions with tetragonally or trigonally-distorted octahedra, the distortion being introduced by static crystal fields, V_{ax}, and odd-parity perturbations in $V_{e\text{-}p}$ in (1). First, we solve (1) in D_{4h} and D_{3d} group symmetries neglecting effects due to H_{ph} and $V_{e\text{-}p}$. Subsequently, the effects of deviations from even axial symmetry, H_{ph} and $V_{e\text{-}p}$, are discussed.

2. Electronic Wavefunctions of ^2E_g and $^2T_{2g}$ of Ti^{3+} in an Axial Crystal Field

Tetragonal Symmetry (D_{4h})

Consider a Ti^{3+} ion at the centre of an octahedral arrangement of six O^{2-} ligand ions. Since the Ti^{3+} ion is finite size, the wavefunctions of the single $3d$ electron extend outwards into the crystal and may overlap those of the neighbouring ligand ions. The eigenfunctions of (1) with the assumption that H_{ph} and $V_{e\text{-}p}$ are neglected are molecular orbitals (MOs) constructed from linear combinations of atomic orbitals in the octahedral basis eigenfunctions of H_0 using the d-orbitals of the central ion and the s- and p-orbitals of the ligands. Orbitals derived from s-states (S_i) and p-states (X_i, Y_i, Z_i) of the i^{th} ligand are classified as σ anti-bonding and π anti-bonding orbitals of e_g symmetry and t_{2g} symmetry [19]. Such MOs take the form

$$\left.\begin{aligned}
|\varepsilon\rangle &= N_\sigma\left[|x^2-y^2\rangle - \frac{c_\sigma}{2}(S_1+S_4-S_2-S_5)\right.\\
&\quad\left. - \frac{c'_\sigma}{2}(-X_1+X_4+Y_2-Y_5)\right]\\
|\theta\rangle &= N_\sigma\left[|2z^2-x^2-y^2\rangle\right.\\
&\quad - \frac{c_\sigma}{\sqrt{12}}(2S_3+2S_6-S_1-S_4-S_2-S_5)\\
&\quad\left. - \frac{c'_\sigma}{\sqrt{12}}(-2Z_3+2Z_6+X_1-X_4+Y_2-Y_5)\right]
\end{aligned}\right\} e_g, \tag{3}$$

$$\left.\begin{aligned}
|\xi\rangle &= N_\pi\left[|yz\rangle - \frac{c_\pi}{2}(Z_2-Z_5+Y_3-Y_6)\right]\\
|\eta\rangle &= N_\pi\left[|zx\rangle - \frac{c_\pi}{2}(X_3-X_6+Z_1-Z_4)\right]\\
|\zeta\rangle &= N_\pi\left[|xy\rangle - \frac{c_\pi}{2}(Y_1-Y_4+X_2-X_5)\right]
\end{aligned}\right\} t_{2g} \tag{4}$$

where N_σ, N_π are the normalization constants and labels 1 to 6 refer to the x, y, and z axes as shown in Fig. 2. The eigenfunctions of (1) which include static tetragonal crystal field $V(A_{1g}(E_g))$, and spin-orbit, $H_{s\text{-}o}$, perturbations are written in terms of the octahedral basis functions in (3) and (4) as

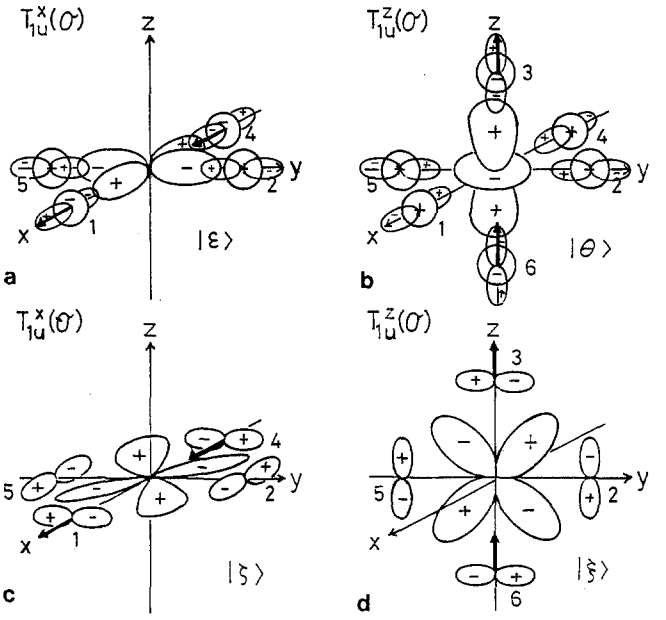

Fig. 2. d-orbitals ($|\varepsilon\rangle$, $|\theta\rangle$, $|\zeta\rangle$, $|\xi\rangle$) and $T_{1u}(\sigma)$ distortions

$$\left.\begin{aligned}
&E_{3/2} \;|\pm 1, \pm\tfrac{1}{2}\rangle\\
&E^1_{1/2} \;|\mp 1, \pm\tfrac{1}{2}\rangle\\
&E^2_{1/2} \;|0, \pm\tfrac{1}{2}\rangle
\end{aligned}\right\} {}^2T_{2g} \tag{5}$$

$$\left.\begin{aligned}
&E_\theta \;|\theta, \pm\tfrac{1}{2}\rangle\\
&E_\varepsilon \;|\varepsilon, \pm\tfrac{1}{2}\rangle
\end{aligned}\right\} {}^2E_g \tag{6}$$

where

$$|\pm 1\rangle = \mp\frac{1}{\sqrt{2}}(|\xi\rangle + i|\eta\rangle)$$
$$|0\rangle = |\zeta\rangle\,. \tag{7}$$

Trigonal Symmetry (D_{3d})

The eigenfunctions of (1) including a static trigonal crystal field, $V(A_{1g}(T_{2g}))$ and $H_{s\text{-}o}$ are written as

$$\left.\begin{aligned}
&E_{3/2} \;|\chi_\pm, \pm\tfrac{1}{2}\rangle\\
&E^1_{1/2} \;|\chi_\mp, \pm\tfrac{1}{2}\rangle\\
&E^2_{1/2} \;|\chi_0, \pm\tfrac{1}{2}\rangle
\end{aligned}\right\} {}^2T_{2g} \tag{8}$$

$$\left.\begin{aligned}
&E_{3/2} \;|u_\pm, \pm\tfrac{1}{2}\rangle\\
&E_{1/2} \;|u_\mp, \pm\tfrac{1}{2}\rangle
\end{aligned}\right\} {}^2E_g \tag{9}$$

where

$$|\chi_\pm\rangle = \mp\frac{1}{\sqrt{2}}(|\eta_X\rangle \pm i|\eta_Y\rangle) \tag{10}$$

$$|\chi_0\rangle = |\eta_Z\rangle,$$

$$|\eta_X\rangle = \frac{1}{\sqrt{6}}(2|\zeta\rangle - |\xi\rangle - |\eta\rangle)$$

$$|\eta_Y\rangle = \frac{1}{\sqrt{2}}(|\xi\rangle - |\eta\rangle) \tag{11}$$

$$|\eta_Z\rangle = \frac{1}{\sqrt{3}}(|\xi\rangle + |\eta\rangle + |\zeta\rangle),$$

and

$$|u_\pm\rangle = \mp\frac{1}{\sqrt{2}}(|\theta\rangle \pm i|\varepsilon\rangle). \tag{12}$$

The separations in energy between $E^1_{1/2}$ and $E_{3/2}$ and between $E^2_{1/2}$ and $E_{3/2}$ for the $^2T_{2g}$ ground state of Ti^{3+} in Al_2O_3 calculated assuming a static trigonal crystal field do not agree with the splittings measured from far infrared absorption spectra [12]. This discrepancy may be removed using the vibronic Hamiltonian in (1) including H_{ph} and V_{e-p} [13].

3. Electron-Phonon Interaction

The electron is assumed to move in a potential $V(q, Q)$ which is a function of electron coordinates q and nuclear coordinates Q and which may be expanded as a power series in Q [20] as

$$V(q,Q) = V_0(q) + \sum_{\Gamma,\gamma}\left(\frac{\partial V}{\partial Q_{\Gamma,\gamma}}\right)Q_{\Gamma,\gamma} + \frac{1}{2}\sum_{\Gamma,\gamma,\Gamma',\gamma'} \times \left(\frac{\partial^2 V}{\partial Q_{\Gamma,\gamma}\partial Q_{\Gamma',\gamma'}}\right)Q_{\Gamma,\gamma}Q_{\Gamma',\gamma'} + \ldots, \tag{13}$$

where $V_0(q)$ is the static octahedral field potential of H_0 in (1), $Q_{\Gamma,\gamma}$ are the collective coordinates of the displacements and Γ, γ are the irreducible representation and component of the group. Assuming that the linear term in the electron–phonon coupling is dominant, the higher order terms in (13) may be neglected and the electron–phonon interaction, V_{e-p}, is written as

$$V_{e-p} = \sum_{\Gamma,\gamma}\frac{\partial V}{\partial Q_{\Gamma\gamma}}Q_{\Gamma\gamma}. \tag{14}$$

The collective coordinates, $Q_{\Gamma\gamma}$, can be classified into even-mode and odd-mode coordinates. The even-modes, for example E_g and T_{2g}, correspond to Jahn-Teller distortions and are dominant. Odd-mode vibrations, T_{1u} and T_{2u}, allow parity-forbidden transitions between the excited and ground states even in the absence of static odd-parity crystal field.

3.1. Jahn-Teller Effect

Tetragonal Symmetry. Consider the Jahn-Teller effect in cubic symmetry. The eigenfunctions of the vibronic Hamiltonian in (1) are products of electronic and vibrational wavefunctions in the Born-Oppenheimer approximation. Since the t_{2g} orbitals of the ground state form π-bonds with the ligands, the Jahn-Teller coupling with the E_g mode is weak [13, 20–22], and does not mix the three wavefunctions $|\xi\rangle$, $|\eta\rangle$ and $|\zeta\rangle$ of the ground state. In contrast, the e_g orbitals of the excited state form σ-bonds with neighbouring ligands as shown by (3), and strong Jahn-Teller coupling is anticipated. The linear Jahn-Teller coupling mixes $|\theta\rangle$ and $|\varepsilon\rangle$ states with Jahn-Teller energy E_{JT} given by $E_{JT} = V^2/2M\omega^2$ ($\sim 3000\,cm^{-1}$), where V is the coupling coefficient, M the ligand mass, and ω the vibration frequency [18]. The anharmonic terms in the potential expansion (warping term) produce three potential minima corresponding to tetragonal distortions along the x, y, and z axes separated by the barrier with height typically in the range 200–600 cm^{-1} [20–22]. When the octahedron is stretched (compressed) along the z-axis, the lowest excited state is $|\theta\rangle$ ($|\varepsilon\rangle$).

Next, consider the Jahn-Teller effect in the presence of an intrinsic tetragonal distortion represented by $V(A_{1g}(E_g))$. If the tetragonal field and the Jahn-Teller distortion have the same sense i.e. a stretch mode, then one of three geometrically equivalent Jahn-Teller distortions is stabilized and the octahedral arrangement of ions is tetragonally distorted. When the tetragonal perturbation has the opposite sense relative to the Jahn-Teller distortion, (e.g., the tetragonal perturbation is a stretch mode and the Jahn-Teller distortion is a compression mode), the distorted octahedron has orthorhombic symmetry. That is, the combined terms of V_{ax} and V_{e-p} in (1) determine the symmetry of the octahedron of Ti^{3+}.

Trigonal Symmetry. The treatment of Jahn-Teller effect in trigonal symmetry is essentially the same as that in tetragonal symmetry. However, the trigonally symmetric crystal field perturbation never stabilizes one of three energetically equivalent vibronic states associated with distortions of the octahedron distorted along the cubic x, y, and z axes. Instead the distortion mixes these vibronic states, splitting them into singlet and doublet states. Furthermore, the magnitude of the trigonal splitting is reduced by the Ham factor, q, relative to that in the absence of a Jahn-Teller effect. If q is fairly small, the trigonal splitting is negligible. This corresponds to the static Jahn-Teller effect in which the complex exhibits tetragonal symmetry. However, when the reduced trigonal splitting is larger than the stabilization energy of the tetragonal distortion as in the case of random strain of E_g symmetry [20–22], the complex will exhibit trigonal symmetry. The lowest excited state of ^2E_g is then given by the wavefunctions $a|\theta\rangle + b|\varepsilon\rangle$ with $|a|^2 + |b|^2 = 1$. Thus, the symmetry and wavefunctions are determined by the competition between the intrinsic trigonal crystal field and the stabilization energy of tetragonal distortion induced by the Jahn-Teller effect.

3.2. Odd-Parity Perturbations

Radiative electric dipole transitions between the excited molecular states, e_g, and the ground molecular states, t_{2g}, are parity forbidden. However, static and dynamic odd-

parity terms of the crystal field, $V(\gamma(\Gamma))$ ($\Gamma = T_{1u}, T_{2u}$) and $V_{e\text{-}p}$ in (1) lift this selection rule by mixing odd-parity wavefunctions into the excited states MOs, e_g and/or the ground states MOs, t_{2g}. We now consider the effects of these odd-parity dynamic and static distortions on the radiative transitions separately.

3.2.1. Dynamic Distortions

Tetragonal Symmetry. The three odd-parity distortions of the octahedral complex transform as the irreducible representations $T_{1u}(\sigma)$, $T_{1u}(\pi)$ and $T_{2u}(\pi)$ of the O_h group [23, 24], σ and π implying that the ligand ion displacements are parallel to and perpendicular to the central-ion/ligand-ion axis, respectively. The $T_{1u}(\sigma)$ odd-parity distortion has three components $T^x_{1u}(\sigma)$, $T^y_{1u}(\sigma)$ and $T^z_{1u}(\sigma)$ with $T^x_{1u}(\sigma)$ and $T^y_{1u}(\sigma)$ being equivalent as examination of Fig. 2 shows. Figure 2 also shows the effects of $T^x_{1u}(\sigma)$ and $T^z_{1u}(\sigma)$ components of the distortion applied to the $|\varepsilon\rangle$, $|\theta\rangle$, $|\zeta\rangle$, and $|\xi\rangle$ MOs. With the $T^x_{1u}(\sigma)$ displacements shown in Fig. 2a, the ligand ion on the negative x-axis of the $|\varepsilon\rangle$ MO, moves nearer to the central ion, and its S_4 and X_4 orbitals are mixed to a greater extent than the orbitals S_1 and X_1 of the ligand ion on the positive x-axis, which moves away from the central ion. This admixture is approximated by a coefficient $[a(S_1 - S_4) - b(X_1 + X_4)]Q_{T_{1u},x}(\sigma)$, where $Q_{T_{1u},x}(\sigma)$ is the normal coordinate of the $T^x_{1u}(\sigma)$ distortion. The $T_{1u}(\sigma)$ odd-parity distortions also affect the $|\xi\rangle$, $|\eta\rangle$, and $|\zeta\rangle$ MOs. The odd wavefunctions of the p-orbitals mixed into the $|\zeta\rangle$ and $|\xi\rangle$ MOs by the $T^x_{1u}(\sigma)$ and $T^z_{1u}(\sigma)$ components with coefficients $c(Y_1+Y_4)Q_{T_{1u},x}(\sigma)$ and $c(Y_3+Y_6)Q_{T_{1u},z}(\sigma)$ are shown in Fig. 2c and d, respectively.

The $T_{1u}(\pi)$ and $T_{2u}(\pi)$ distortions cause similar admixtures of odd wavefunctions in the $|\theta\rangle$, $|\varepsilon\rangle$, $|\xi\rangle$, $|\eta\rangle$, and $|\zeta\rangle$ MOs. When the $T^z_{1u}(\pi)$ component perturbs the $|\xi\rangle$ MO, the π-bonding axis between the central ion and the 2nd and 5th ligands bends slightly towards the y axis as is shown in Fig. 3b. This effect is approximated by an admixture coefficient $c'(Y_2 + Y_5)Q_{T_{1u},z}(\pi)$. $T_{2u}(\pi)$ odd-parity distortions mix the same odd-parity wavefunctions of p-orbitals into the t_{2g} MOs but with different phase from that induced by $T_{1u}(\pi)$ distortion. The odd-parity admixture induced in the $|\xi\rangle$ MO by $T^z_{2u}(\pi)$ is $-c''(Y_2 + Y_5)Q_{T_{2u},z}(\pi)$ (Fig. 3d). The admixture of the odd wavefunctions of the s-orbitals into the $|\theta\rangle$ and $|\varepsilon\rangle$ MOs is negligible because these MOs are composed of σ-bonding orbitals, while the admixture of p-orbitals into the $|\theta\rangle$ and $|\varepsilon\rangle$ MOs are affected by $T_{1u}(\pi)$ and $T_{2u}(\pi)$ distortions. When the $T^z_{1u}(\pi)$ component perturbs the $|\varepsilon\rangle$ MO, the σ-bonding axes of 1st, 2nd, 4th, and 5th ligand ions bend slightly toward the z-axis. Then, the induced odd-parity wavefunction is approximately $b'(Z_1 + Z_4 - Z_2 - Z_5)Q_{T_{1u},z}(\pi)$. The results for all appropriate wavefunctions in octahedral symmetry are summarized in Table 2.

Trigonal Symmetry. We apply the odd-parity distortions to Ti^{3+} ions occupying trigonal crystal field sites in, for example Al_2O_3 where the crystal structure is axially symmetric about the c axis. The new axes are chosen to be $X \| \langle \bar{1}\bar{1}2 \rangle$, $Y \| \langle 1\bar{1}0 \rangle$ and $Z \| \langle 111 \rangle$. The components of

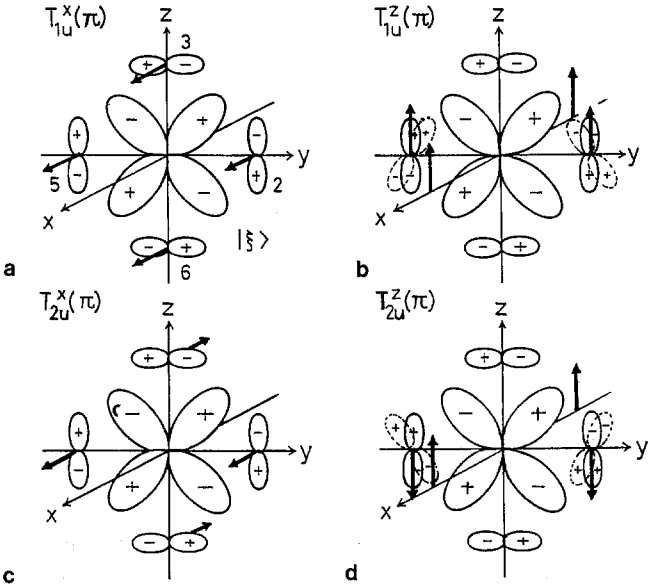

Fig. 3. d-orbital ($|\xi\rangle$) and $T_{1u}(\pi)$ and $T_{2u}(\pi)$ distortions

the $T_{1u}(\sigma)$, $T_{1u}(\pi)$ and $T_{2u}(\pi)$ odd-parity distortions and odd-parity MOs are transformed from octahedral to trigonal bases. The transformed distortions and MOs have the same form as the $^2T_{2g}$ in (11) and the subscripts ($\gamma = X, Y, Z$) of $Q_{\Gamma,\gamma}$ replace $\gamma = x, y, z$ in the octahedral basis. The odd-parity wavefunctions induced into the ground states $|\eta_X\rangle$, $|\eta_Y\rangle$, and $|\eta_Z\rangle$ by odd-parity trigonal perturbations calculated using Table 2 are summarized in Table 3. The X, Y, and Z components of $T_{2u}(\pi)$ do not create odd-terms of ligand p-orbitals in $|\eta_X\rangle$, $|\eta_Y\rangle$, and $|\eta_Z\rangle$, respectively. The eigenfunctions of the ground state in trigonal symmetry are $|\chi_\pm\rangle = \mp\frac{1}{\sqrt{2}}(|\eta_X\rangle \pm i|\eta_Y\rangle)$ and $|\chi_0\rangle = |\eta_Z\rangle$, and the odd-parity wavefunctions induced into $|\chi_\pm\rangle$ and $|\chi_0\rangle$ are reproduced using Table 3.

3.2.2. Static Distortions

Odd-parity static distortions correspond to irreducible displacement coordinates in the absence of the kinetic energy term in H_{ph}. If the symmetry of Ti^{3+}-doped crystals remains as that of the pure crystals, the static distortions agree with the intrinsic odd-parity crystal field components deviated from cubic symmetry in Table 1, that is, the z (Z) component of the odd-parity dynamic distortions for the tetragonal (trigonal) symmetry. However, if the distortions of the octahedron produced by terms in $V_{e\text{-}p}$ are different from the intrinsic crystal field, they must be localized distortions. The x, y, and z (X, Y, and Z) components of such distortions for tetragonal (trigonal) symmetry have different electron-phonon coupling. However, the induced odd-parity wavefunctions are the same as those by odd-parity dynamic distortions.

4. Polarization of Luminescence and Selection Rules

The emission spectrum of Ti^{3+} ions consists of the zero-phonon lines and the broad band. The zero-phonon tran-

Table 2. Odd-parity wavefunctions of ligand orbitals mixed into MOs $|\varepsilon\rangle$, $|\theta\rangle$, $|\xi\rangle$, $|\eta\rangle$, and $|\zeta\rangle$ by lattice vibrations $T_{1u}(\sigma)$, $T_{1u}(\pi)$, and $T_{2u}(\pi)$

Vibration	MO				
	$\|\varepsilon\rangle$	$\|\theta\rangle$	$\|\xi\rangle$	$\|\eta\rangle$	$\|\zeta\rangle$
$T_{1u}(\sigma)$					
x	$a(S_1-S_4)-b(X_1+X_4)$	$\frac{1}{\sqrt{3}}[-a(S_1-S_4)+b(X_1+X_4)]$	0	$c(Z_1+Z_4)$	$c(Y_1+Y_4)$
y	$-a(S_2-S_5)+b(Y_2+Y_5)$	$\frac{1}{\sqrt{3}}[-a(S_2-S_5)+b(Y_2+Y_5)]$	$c(Z_2+Z_5)$	0	$c(X_2+X_5)$
z	0	$\frac{1}{\sqrt{3}}[2a(S_3-S_6)-2b(Z_3+Z_6)]$	$c(Y_3+Y_6)$	$c(X_3+X_6)$	0
$T_{1u}(\pi)$					
x	$-b'(X_2+X_5)$	$\frac{b'}{\sqrt{3}}[-(X_2+X_5)+2(X_3+X_6)]$	0	$c'(Z_3+Z_6)$	$c'(Y_2+Y_5)$
y	$b'(Y_1+Y_4)$	$\frac{b'}{\sqrt{3}}[-(Y_1+Y_4)+2(Y_3+Y_6)]$	$c'(Z_3+Z_6)$	0	$c'(X_1+X_4)$
z	$b'[(Z_1+Z_4)-(Z_2+Z_5)]$	$-\frac{b'}{\sqrt{3}}[(Z_1+Z_4)+(Z_2+Z_5)]$	$c'(Y_2+Y_5)$	$c'(X_1+X_4)$	0
$T_{2u}(\pi)$					
x	$-b''(X_2+X_5)$	$\frac{b''}{\sqrt{3}}[-(X_2+X_5)-2(X_3+X_6)]$	0	$-c''(Z_3+Z_6)$	$c''(Y_2+Y_5)$
y	$-b''(Y_1+Y_4)$	$\frac{b'}{\sqrt{3}}[(Y_1+Y_4)+2(Y_3+Y_6)]$	$c''(Z_3+Z_6)$	0	$-c''(X_1+X_4)$
z	$b''[(Z_1+Z_4)+(Z_2+Z_5)]$	$\frac{b''}{\sqrt{3}}[-(Z_1+Z_4)+(Z_2+Z_5)]$	$-c''(Y_2+Y_5)$	$c''(X_1+X_4)$	0

Table 3. Odd-parity wavefunctions of ligand orbitals mixed into MOs of the ground state $|\eta_X\rangle$, $|\eta_Y\rangle$, $|\eta_Z\rangle$ on trigonal basis by lattice vibration $T_{1u}(\sigma)$, $T_{1u}(\pi)$, and $T_{2u}(\pi)$

Vibration	MO		
	$\|\eta_X\rangle$	$\|\eta_Y\rangle$	$\|\eta_Z\rangle$
$T_{1u}(\sigma)$			
X	$\frac{1}{6}[-2(X_2+X_3)-2(Y_1+Y_3)+(Z_1+Z_2)]$	$\frac{1}{2\sqrt{3}}[-2(X_3-Y_3)+(Z_1-Z_2)]$	$\frac{1}{3\sqrt{2}}[(-X_2+2X_3)+(-Y_1+2Y_3)-(Z_1+Z_2)]$
Y	$\frac{1}{2\sqrt{3}}[-2(X_2-Y_1)-(Z_1-Z_2)]$	$-\frac{1}{2}2(Z_1+Z_2)$	$\frac{1}{\sqrt{6}}[(-X_2+Y_1)+(Z_1-Z_2)]$
Z	$\frac{1}{3\sqrt{2}}[(2X_2-X_3)+(2Y_1-Y_3)-(Z_1+Z_2)]$	$-\frac{1}{\sqrt{6}}[(X_3-Y_3)+(Z_1-Z_2)]$	$\frac{1}{3}[(X_2+X_3)+(Y_1+Y_3)+(Z_1+Z_2)]$
$T_{1u}(\pi)$			
X	$\frac{1}{3}[(Z_3+Z_6)-2(X_1+X_4)-2(Y_1+Y_5)]$	$-\frac{1}{\sqrt{3}}[(X_1+X_4)-(Y_2+Y_5)]$	$-\frac{1}{3\sqrt{2}}[2(Z_3+Z_6)-(X_1+X_4)-(Y_2+Y_5)]$
Y	$-\frac{1}{\sqrt{3}}[(X_1+X_4)-(Y_2+Y_5)]$	$-(Z_3+Z_6)$	$-\frac{1}{\sqrt{6}}[(X_1+X_4)-(Y_2+Y_5)]$
Z	$-\frac{1}{3\sqrt{2}}[2(Z_3+Z_6)-(X_1+X_4)-(Y_2+Y_5)]$	$-\frac{1}{\sqrt{6}}[(X_1+X_4)-(Y_2+Y_5)]$	$\frac{2}{3}[(X_1+X_4)+(Y_2+Y_5)+(Z_3+Z_6)]$
$T_{2u}(\pi)$			
X	0	$-\frac{1}{\sqrt{3}}[(X_1+X_4)+(Y_2+Y_5)+(Z_3+Z_6)]$	$\frac{1}{\sqrt{2}}[(X_1+X_4)-(Y_2+Y_5)]$
Y	$\frac{1}{\sqrt{3}}[(X_1+X_4)+(Y_2+Y_5)+(Z_3+Z_6)]$	0	$-\frac{1}{\sqrt{6}}[2(Z_3+Z_6)-(X_1+X_4)-(Y_2+Y_5)]$
Z	$-\frac{1}{\sqrt{2}}[(X_1+X_4)-(Y_2+Y_5)]$	$\frac{1}{\sqrt{6}}[2(Z_3+Z_6)-(X_1+X_4)-(Y_2+Y_5)]$	0

sition between the excited state $|^2E_g\chi, \alpha\rangle$ and the ground state $|^2T_{2g}\chi', \alpha'\rangle$ where χ and χ' are orbital components of ^2E_g and $^2T_{2g}$ and α and α' are spin states is allowed by the intrinsic static crystal field, V_{ax} and the static distortion, whereas the broad band is allowed by static and dynamic distortions of the crystal field. The electric dipole moment operator, $D = -e\mathbf{r}\cdot\mathbf{E}$, operates only on the orbital states. The matrix element $\langle^2E_g\chi, \alpha|D|^2T_{2g}\chi', \alpha\rangle$ of the electric dipole transition induced by the odd-parity perturbations $V(T_{1u})$, $(V(T_{2u}))$ are given by

$$\frac{\langle^2E_g\chi, \alpha|D|^2\Gamma_u\gamma'\alpha\rangle\langle^2\Gamma_u\gamma, \alpha|V(T_{1u})|^2T_{2g}\chi', \alpha\rangle}{E(^2T_{2g}) - E(^2\Gamma_u)} + \frac{\langle^2E_g\chi, \alpha|V(T_{1u})|^2\Gamma_u'\gamma', \alpha\rangle\langle^2\Gamma_u'\gamma', \alpha|D|^2T_{2g}\chi', \alpha\rangle}{E(^2E_g) - E(^2\Gamma_u')}, \quad (15)$$

where $E(^2T_{2g})$, $E(^2E_g)$ and $(E(^2\Gamma_u), E(^2\Gamma_u'))$ are energy levels of the ground, excited and intermediate states [25], respectively and the components of the intermediate states, γ and γ' are given in Table 2 and 3. The first and second terms in (15) represent the radiative transitions due to mixing odd terms from ligand p-orbitals into $^2T_{2g}$ and mixing odd-parity wavefunctions of the ligand s- and p-orbitals for ^2E_g by odd-parity perturbations, respectively. The relative magnitudes of the matrix elements determined using vibronic wavefunctions are the same as those calculated using the purely electronic wavefunctions because the contribution of the nuclear wavefunctions to the electric dipole matrix element takes the form of the reduction factor. Therefore, the matrix elements are calculated using the electronic wavefunctions of the ground state, ($|\xi\rangle$, $|\eta\rangle$, $|\zeta\rangle$ or $|\pm1\rangle$, $|0\rangle$) and ($|\eta_X\rangle$, $|\eta_Y\rangle$, $|\eta_Z\rangle$ or $|\chi_\pm\rangle$, $|\chi_0\rangle$), and those of the lowest

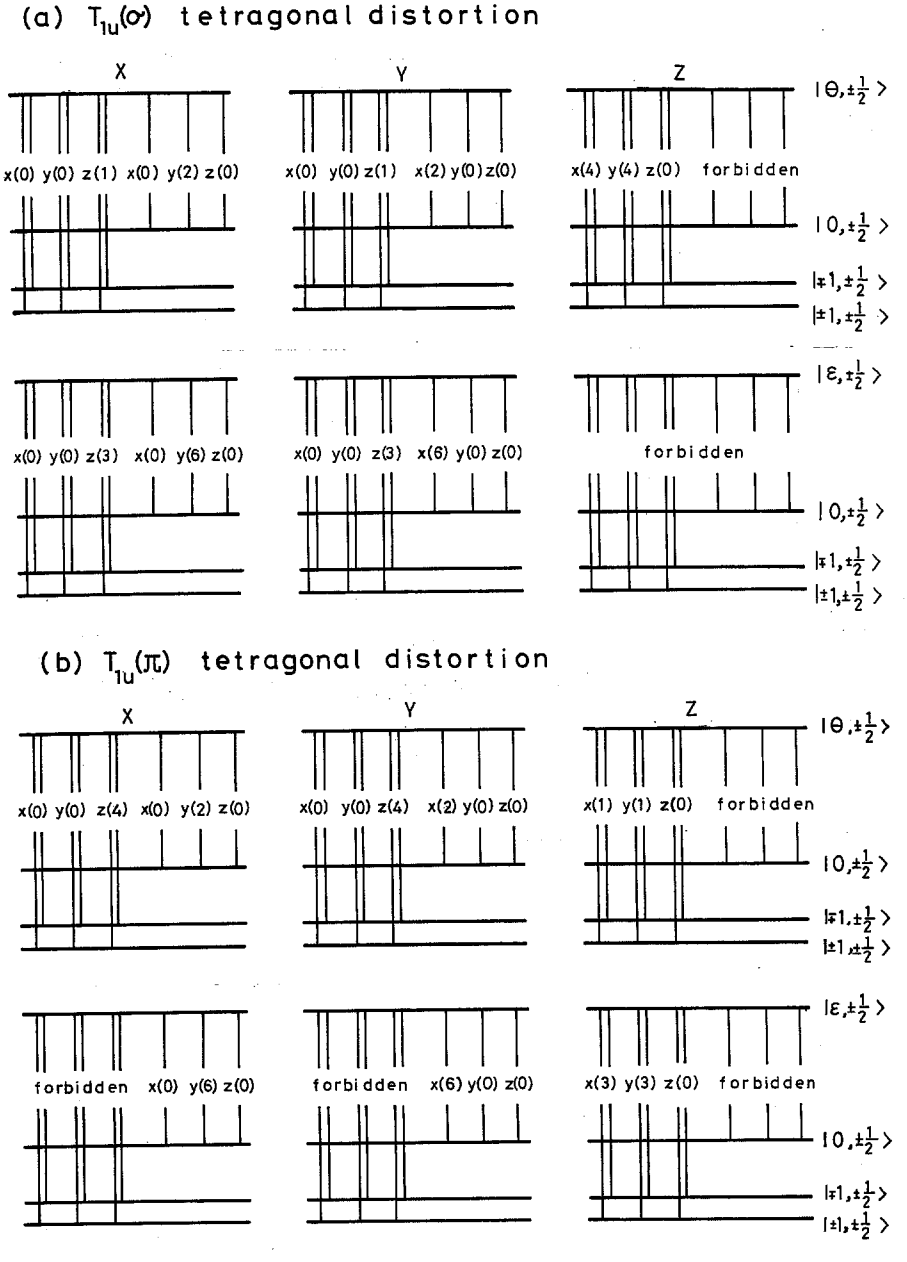

Fig. 4a, b. Polarizations and relative intensities of the emission induced by **a** $T_{1u}(\sigma)$ distortion, **b** $T_{1u}(\pi)$ distortion in tetragonal symmetry. The letters x y, and z represent the x y, and z components of polarization in tetragonal symmetry. The numbers in parentheses represent the relative intensity

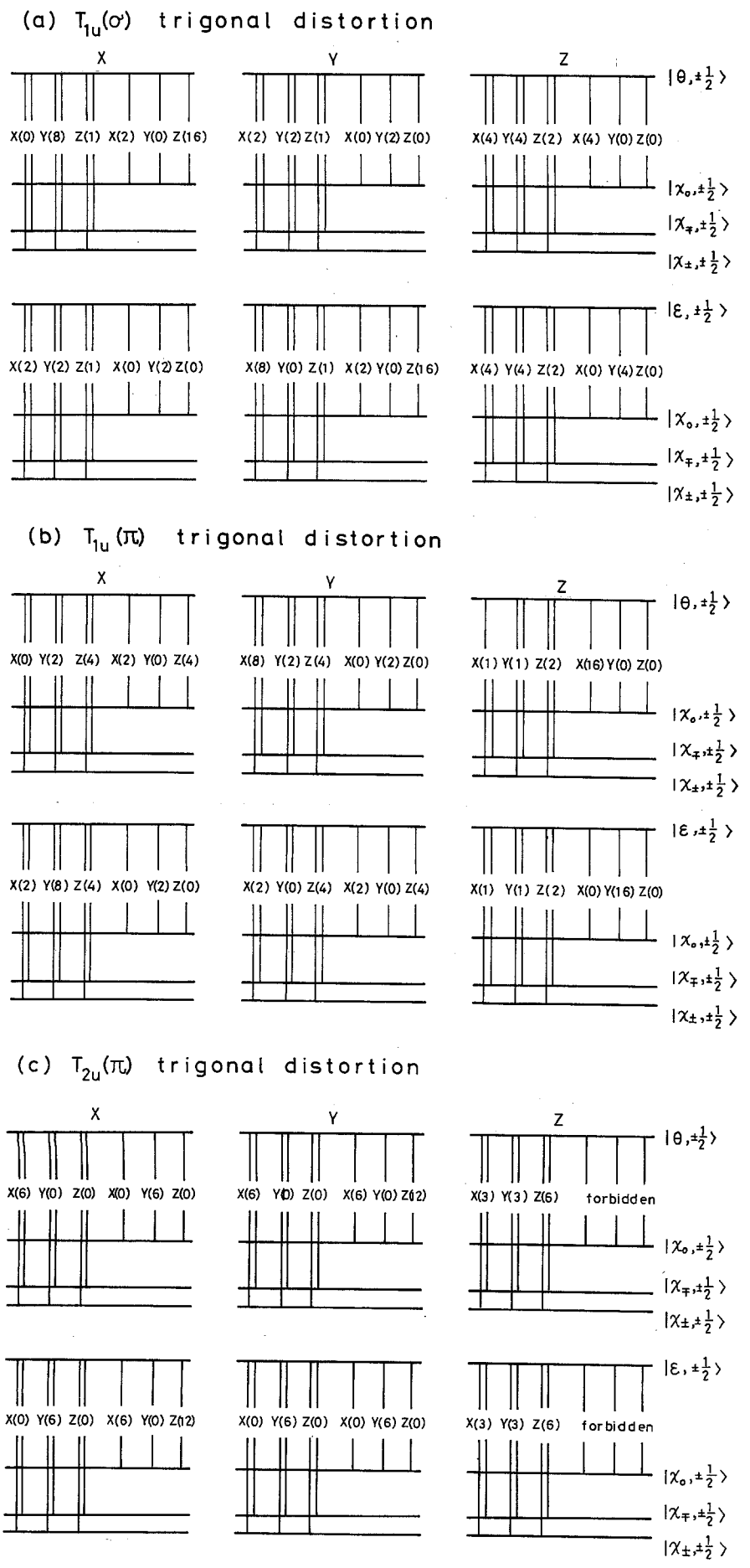

Fig. 5a–c. Polarizations and relative intensities of the emission induced by **a** $T_{1u}(\sigma)$ distortion, **b** $T_{1u}(\pi)$ distortion, **c** $T_{2u}(\pi)$ distortion in trigonal symmetry. The letters X Y, and Z represent the X Y, and Z components of polarization in trigonal symmetry. The numbers in parentheses represent the relative intensity

excited state, ($|\theta\rangle$, $|\varepsilon\rangle$) and $\mp\frac{1}{\sqrt{2}}(|\theta\rangle \pm i|\varepsilon\rangle)$ corresponding to tetragonal or trigonal symmetry, respectively.

Tetragonal Symmetry. As shown in Table 1, the intrinsic static crystal field has only the z-component of T_{1u}, $V(A_{2u}(T_{1u}))$, in tetragonal symmetry. Although the odd-parity wavefunctions induced by $T_{2u}(\pi)$ dynamic distortion has different phase from those induced by $T_{1u}(\pi)$, the transition probabilities and polarizations produced by $T_{1u}(\pi)$ and $T_{2u}(\pi)$ are the same. Therefore, only the relative values of the matrix elements $\langle\chi|D|\chi'\rangle$ ($\chi = \theta, \varepsilon$, and $\chi' = \xi, \eta, \zeta$) produced by $T_{1u}(\pi)$ and $T_{1u}(\pi)$ odd-parity distortions in the tetragonal symmetry are calculated using Table 2. For example, the matrix element $\langle\theta|D|\xi\rangle$ produced by the y component of $T_{1u}(\sigma)$ in (15) is given by

$$\begin{aligned}\langle\theta|D|\xi\rangle &= \alpha\langle\theta|D|\Gamma_u\gamma\rangle + \beta\langle\Gamma'_u\gamma'|D|\xi\rangle \\ &= \alpha\langle\theta|D|c(Z_2+Z_5)\rangle \\ &\quad + \beta\langle -a(S_2-S_5)+b(Y_2+Y_5)|D|\xi\rangle . \qquad (16)\end{aligned}$$

The first and second terms, respectively, correspond to the transitions between the even-MOs of the central d-orbital and ligand orbitals in E_g and the odd-MOs of ligand p-orbitals in T_{2g} and between the odd-MOs of ligand s- and p-orbitals in E_g and the even-MOs of the central d-orbitals and ligand p-orbitals in T_{2g}. The values of the two terms are different, but both are non-zero for $D\|z$. Then, the emission due to the transition from $|\theta\rangle$ to $|\xi\rangle$ induced by the y component of $T_{1u}(\sigma)$ distortion is polarized along the z direction. The relative intensities and polarizations of the emission produced by $T_{1u}(\sigma)$ and $T_{1u}(\pi)$ distortions are shown in Fig. 4a, b.

The z-component of $T_{1u}(\sigma)$ distortion does not allow the transition $\langle\theta|D|0\rangle$, $\langle\varepsilon|D|0\rangle$ and $\langle\varepsilon|D|\pm 1\rangle$, whereas the z-component of $T_{1u}(\pi)$ allows the transitions $\langle\theta|D|\pm 1\rangle$ and $\langle\varepsilon|D|\pm 1\rangle$: the transitions $\langle\theta|D|0\rangle$ and $\langle\varepsilon|D|0\rangle$ are still forbidden. The remarkably different point between $T_{1u}(\sigma)$ and $T_{1u}(\pi)$ is that transitions $\langle\varepsilon|D|\pm 1\rangle$ are still forbidden for both x and y components of $T_{1u}(\pi)$ distortion.

Trigonal Symmetry. The symmetry of the ground state of Ti^{3+} in Al_2O_3 is trigonal [13]. However, the symmetry of the excited state which is determined by the competition of the static trigonal crystal field and Jahn-Teller effect has not been established experimentally. First, the matrix elements of the transitions $\langle\theta|D|\chi_i\rangle$ and $\langle\varepsilon|D|\chi_i\rangle$ ($i = \pm, 0$), respectively, are calculated in the same way as for tetragonal symmetry. If the symmetry of the excited state is trigonal, the transition probabilities are changed to $|\langle u_\pm|D|\chi_i\rangle|^2$ ($i = \pm, 0$) which is given by the average of $|\langle\theta|D|\chi_i\rangle|^2$ and $|\langle\varepsilon|D|\chi_i\rangle|^2$. The transition probabilities, $|\langle\theta|D|\chi_\pm\rangle|^2$, are also given by the average of $|\langle\theta|D|\eta_X\rangle|^2$ and $|\langle\theta|D|\eta_Y\rangle|^2$. The relative intensities and polarizations of the emission induced by $T_{1u}(\sigma)$, $T_{1u}(\pi)$ and $T_{2u}(\pi)$ distortions are shown in Fig. 5a–c. The selection rule derived from the Z-component of the $T_{2u}(\pi)$ distortion in the trigonal symmetry is that the polarization of the transitions $\langle\theta|D|\chi_\pm\rangle$ and $\langle\varepsilon|D|\chi_\pm\rangle$ are $I_X : I_Y : I_Z = 1 : 1 : 2$ and the transitions of $\langle\theta|D|\chi_0\rangle$ and $\langle\varepsilon|D|\chi_0\rangle$ are still forbidden.

5. Conclusions

We have discussed the radiative transitions of Ti^{3+} in static axial crystal field in terms of the wavefunctions of the ground and excited states. These wavefunctions are represented by the eigenfunctions of the vibronic Hamiltonian including intrinsic static crystal field, spin-orbit interaction and electron-phonon interaction. The radiative decay occurs through mixing of odd-parity wavefunctions into the even-parity ground and excited states by odd-parity perturbations of T_{1u} and T_{2u}. The relative intensities and polarizations of Ti^{3+} emission in tetragonal and trigonal symmetries have been calculated using the odd-parity wavefunctions.

The zero-phonon line emission is allowed by the intrinsic static crystal field and the static distortion, whereas the braod-band is allowed by the intrinsic static crystal field and both static and dynamic distortions. As the transition due to the dynamic distortion is associated with odd-parity phonon emission or absorption, which static or dynamic distortion contributes to the broad-band transitions is determined by the temperature dependence of the fluorescence lifetime and total intensity of the broad-band. In subsequent papers, the polarizations of emission spectra of Ti^{3+} doped YAP, YAG, and Al_2O_3 observed at 10 K [26] and the temperature dependence of the fluorescence lifetime and total intensity of the broad bands of Ti^{3+} in these crystals [27] will be reported and compared with the results obtained in this paper.

Acknowledgements. M. Yamaga is indebted to the INAMORI foundation for financial support. B. Henderson and K. P. O'Donnell are indebted to the Science and Engineering Research Council for the support of the research program of which this work forms a part.

References

1. J.C. Walling, O.G. Peterson, H.P. Jenssen, R.C. Morris, E.W. O'Dell: IEEE J. QE-**16**, 1302 (1980)
2. B. Struve, G. Huber: Appl. Phys. B **30**, 117 (1983)
3. J. Drube, B. Struve, G. Huber: Opt. Commun. **50**, 45 (1984)
4. S.T. Lai, B.H.T. Chai, M. Long, R.C. Morris: IEEE J. QE-**22**, 1931 (1986)
5. W. Kolbe, K. Petermann, G. Huber: IEEE J. QE-**21**, 1596 (1985)
6. O. Pilla, E. Galvanetto, M. Montagna, G. Viliani: Phys. Rev. B **38**, 3477 (1988)
7. P.F. Moulton: Opt. News **8**, 9 (1982)
8. P.F. Moulton: J. Opt. Soc. Am. B **3**, 125 (1986)
9. W.R. Rapoport, C.P. Khattak: A.B. Budgor, L. Esterowitz, L.G. DeShazer (eds.) *Tunable Solid-State Lasers II*, Springer Ser. Opt. Sci. Vol. 52 (Springer, Berlin, Heidelberg 1986) pp. 212–217
10. K.L. Schepler: In Ref. [9] pp. 235–239
11. F. Bantien, P. Albers, G. Huber: J. Lumin. **36**, 363 (1987)
12. E.D. Nelson, J.Y. Wong, A.L. Schawlow: Phys. Rev. **156**, 298 (1967)
13. R.M. Macfarlane, J.Y. Wong, M.D. Sturge: Phys. Rev. **166**, 250 (1968)
14. P.F. Moulton: In *Tunable Paramagnetic-Ion Lasers*, ed. by M. Bass, M.L. Stitch, Laser Handbook Vol. 5 (North-Holland, Amsterdam 1985) p. 203

15. C.E. Byvik, A.M. Buoncristiani, S.J. McMurray, M. Kokta: In Ref. [9] pp. 242–246
16. P. Albers, E. Stark, G. Huber: J. Opt. Soc. Am. B **3**, 134 (1986)
17. S. Sugano, Y. Tanabe, H. Kamimura: *Multiplets of Transition Metal Ions in Crystal* (Academic, New York 1970)
18. D.S. McClure: J. Chem. Phys. **36**, 2757 (1962)
19. J.H.M. Thornley, C.G. Windsor, J. Owen: Proc. R. Soc. London A **284**, 252 (1964)
20. M.D. Sturge: In *The Jahn-Teller Effect in Solids*, ed. by F. Seitz, D. Turnbull, H. Ehrenriech, Solid State Physics, Vol. 20 (Academic, New York 1968) p. 91
21. F.S. Ham: Phys. Rev. A **138**, 1727 (1965)
22. S. Geschwind (ed.): *Electron Paramagnetic Resonance* (Plenum, New York 1972) Chap. 1
23. H. Yoshioka, N. Sugimoto, M. Yamaga: J. Phys. Soc. Jpn. **54**, 3990 (1985)
24. M. Yamaga, B. Henderson, K.P. O'Donnell: J. Lumin. **46**, 397 (1990)
25. C.T. Ballhausen, H.B. Gray: *Molecular Orbital Theory* (Benjamin/
Cummings, London 1964) Chap. 8
26. M. Yamaga, B. Henderson, K.P. O'Donnell, F. Rasheed, Y.Gao, B. Cockayne: Appl. Phys. B (to be published)
27. M. Yamaga, Y. Gao, F. Rasheed, K.P. O'Donnell, B. Henderson, B. Cockayne: Appl. Phys. B (to be published)